Video Article

Implementation of a Reference Interferometer for Nanodetection

Serge Vincent*[1], Wenyan Yu*[1], Tao Lu[1]

[1]Department of Electrical and Computer Engineering, University of Victoria

*These authors contributed equally

Correspondence to: Tao Lu at taolu@ece.uvic.ca

URL: https://www.jove.com/video/51133
DOI: doi:10.3791/51133

Keywords: Physics, Issue 86, biosensor, nanodetector, optical microcavity, whispering-gallery mode cavity, reference interferometer, nanoparticles, free spectral range (FSR)

Date Published: 4/26/2014

Citation: Vincent, S., Yu, W., Lu, T. Implementation of a Reference Interferometer for Nanodetection. *J. Vis. Exp.* (86), e51133, doi:10.3791/51133 (2014).

Abstract

A thermally and mechanically stabilized fiber interferometer suited for examining ultra-high quality factor microcavities is fashioned. After assessing its free spectral range (FSR), the module is put in parallel with a fiber taper-microcavity system and then calibrated through isolating and eliminating random shifts in the laser frequency (*i.e.* laser jitter noise). To realize the taper-microcavity junction and to maximize the optical power that is transferred to the resonator, a single-mode optical fiber waveguide is pulled. Solutions containing polystyrene nanobeads are then prepared and flown to the microcavity in order to demonstrate the system's ability to sense binding to the surface of the microcavity. Data is post-processed via adaptive curve fitting, which allows for high-resolution measurements of the quality factor as well as the plotting of time-dependent parameters, such as resonant wavelength and split frequency shifts. By carefully inspecting steps in the time-domain response and shifting in the frequency-domain response, this instrument can quantify discrete binding events.

Video Link

The video component of this article can be found at https://www.jove.com/video/51133/

Introduction

Research interest has risen significantly on the use of whispering-gallery mode (WGM) microcavities for the purpose of nanodetection and biosensing[1-8]. This involves ultra-high quality factor (Q) optical cavities that are proficient in identifying miniscule biological particles, down to the single-protein level[2]. That is, monitoring shifts in resonance and split frequency for transmission with extraordinary sensitivity[9-11] can be enabled by the cavity's confinement of light energy within a small mode volume. Variations in the optical properties of a resonator are the cause of these shifts, which in turn originate from the binding of discrete molecules or nanoparticles. A less sophisticated example of a three-dimensional WGM structure for such applications is a silica microsphere, which can be fabricated with a near atomically smooth surface by simply ablating a drawn optical fiber using a CO_2 laser. As is known, high Q-factors on the order of 10^9 can be attained[1].

The resonant frequency of a microcavity is conventionally monitored by scanning the optical frequency of a tunable laser source while simultaneously photo-detecting the optical transmission that is captured on an oscilloscope. An inherent drawback of this technique is the uncertainty associated with the location of drops in the transmission that arises from fluctuating laser wavelength or laser jitter. To overcome this complication, an interferometer can be used alongside a microcavity to produce a reference signal to cancel the laser jitter and increase the observed sensitivity[2]. Light input is split into two optical paths: the reference beam that passes through the interferometer (with a free spectral range or FSR large enough to prevent the laser from jittering past one FSR frequency spacing during measurement) and the detection beam that interacts with the WGM microresonator. This feature streamlines experiments in comparison to more advanced configurations, such as that of WGM sensing entailing the combination of a distributed feedback laser (DFB) and periodically poled lithium niobate (PPLN) doubler[12]. In this publication, an interferometer technique for ultra-high quality factor microcavity based monitoring of nanoscale matter is described[3]. The setup and data acquisition procedures that are required to accomplish this are outlined, illustrating how cavity quality factor can be determined through reference interferometry.

Protocol

1. Reference Interferometer Construction and FSR Measurement

1. Construction
    1. Create an open-top acrylic box. This structure should be large enough to fit snugly into a 16 in x 16 in x 16 in Styrofoam box.

2. Fabricate a 3-stage shelving unit to house optical components, which will sit in the open-top acrylic box and will be completely enclosed by the Styrofoam box for thermal isolation. Two elevated holes on the Styrofoam box must be present to allow for fibers to enter and exit the entire enclosure.
3. On the 3rd stage: One output fiber from the 3 dB directional coupler should be clamped to a polarization controller which in turn leads to an input port of a separate 3 dB directional coupler.
4. On the 2nd stage: Form a loop with roughly 16 feet of the optical fiber originating from the other output port of the first 3 dB directional coupler. Direct this fiber to the remaining input port of the second 3 dB directional coupler on the 3rd stage.
5. Fill the acrylic box with 50% shaved ice mixed with 50% liquid water, as to fashion an ice bath and consequently maintain the temperature of the optical components near 0 °C.

2. FSR Measurement
    1. Set up the probe laser at the desired wavelength. Employ a function generator such that its output is connected to a 3 dB power splitter. One of the outputs from the 3 dB splitter must be connected to the oscilloscope for monitoring purposes and the other output is to be used to directly tune the frequency of the laser.
    2. Feed the laser output as the input to the 1st 3 dB directional coupler.
    3. The two outputs of the 2nd 3 dB directional coupler are to carry photomixed signals to the balanced photodetector (BPD). Finally, connect the output cable of the BPD to a channel input of the oscilloscope.
    4. Linearly scan the laser frequency by supplying the laser module with a ramp signal generated from the waveform generator (with a peak-to-peak voltage of 1 V and scan frequency of 100 Hz). The output signal from the BPD will become sinusoidal on the oscilloscope.
    5. Tune the polarization controller as to maximize the peak-to-peak voltage of the sinusoidal waveform.
    6. To measure the FSR, configure the laser for continuous wave output by setting the waveform generator to DC mode. Tune the waveform generator voltage such that the transmitted signal from the BPD fluctuates around 0 V (*i.e.* the quadrature point). Inspect the output signal using an electrical spectrum analyzer. The monitored signal should appear as a sinc-square function, where the location of the first zero nearest the global maximum (at zero frequency) corresponds to the FSR. To minimize the measurement noise, set the electrical spectrum analyzer to averaging mode.

2. Fiber Pulling[13]

Preamble: The goal of this procedure is to approximately match the phase of photons travelling in the taper to those of the microcavity so that efficient coupling can occur. As the fiber is pulled, the central section that lies between the two clamps will transition from supporting a single mode within a regular fiber, to multiple modes within a waveguide formed by the original silica cladding becoming the core and air becoming the cladding, and then to a single mode. The silica core of the fiber will virtually vanish in the central section, wherein temporarily satisfied multimode propagation conditions will be counteracted by the continual shrinking of the fiber diameter.

1. Fix the fiber holder to the motorized translational stage.
2. Connectorize two sections of optical fiber with FC/APC connectors on one end of each section. Remove the buffer coating from the unconnected ends with a fiber stripper, clean them with acetone first and then isopropanol, cleave the end facets, and fusion splice them together.
3. To monitor the loss in the taper, connect a probe laser in constant power mode to one end of the fiber while the other end of the fiber is connected to a photodetector (PD). The output of the PD must be connected to an oscilloscope. Adjust the oscilloscope settings as to measure the PD output voltage, which is proportional to the transmitted laser power.
4. Record the initial value of the PD output voltage and continue to monitor it until step 2.9.
5. Clamp the fiber to the fiber holder and image the fiber with an optical microscope.
6. Release hydrogen such that it begins to flow near the taper, waiting for air to exit the tube and for the pressure of the channel to stabilize. Once the flow rate for the hydrogen gas reaches 110 ml/min, ignite it near the outlet with a lighter to heat the fiber.
7. Using a custom LabVIEW program, linearly pull the fiber. Note that during the pulling process, the fiber core gradually vanishes whilst multiple cladding modes become dominant in guiding the light through the tapered fiber section. The transmitted intensity through the optical fiber should oscillate due to multimode interference.
8. Continue pulling the fiber to reduce the fiber taper width until it only supports a single cladding mode. Once the transmitted intensity ceases to vary, stop pulling the fiber.
9. Release the fiber holder from the translation stage and secure it near the piezoelectric stage.

3. Preparation and Delivery of Solutions

1. Prepare 10 pM, 1 pM, and 100 fM solutions composed of 50 nm radius monodisperse polystyrene microspheres in Dulbecco's phosphate buffered saline (DPBS). Additionally, create a pure DPBS solution.
2. Place the solutions in a centrifuge, stagger their positions within it for balance purposes, and initiate a 30 min spinning cycle.
3. Upon completion, securely place the solutions in a desiccator, evacuate it, and bombard the solutions with ultrasound waves for 30 min.
4. Remove the solutions and set them aside near the experiment setup.
5. Build a stand for a small fluid delivery system.
    1. Upon cleaning two ferrules, insert syringe tips onto both ends of a microtubule segment and screw on the ferrules to the syringe tips. Individually connect one of the ferrules to a third syringe tip and the other to the Luer lock fitting of a barrel-plunger assembly.
    2. Fasten the exposed syringe tip to the stand and prop it behind the sample. The fluids should be able to flow onto the sample without significant spillage.

6. In terms of Section 5 of the Protocol, load the barrel with an appropriate solution and manually inject it through the microfluidic system during experiment.

4. System Configuration and Interconnections

1. Connect the probe laser to a 10 dB directional coupler. The coupled port is connected to the input port of the reference interferometer while the transmitted port is connected to a polarization controller followed by the tapered fiber.
2. Refocus the microscope objectives to acquire two sharp images of the fiber taper.
3. Connect the output of the tapered fiber to a PD. The output of this PD should be attached to a different channel input of the oscilloscope.
4. Mount the sample on the nanopositioner and make coarse adjustments to displace it so that it is proximate to the center of the fiber taper.
5. Inject DPBS to the sample. Make coarse adjustments such that the fiber taper comes into view of the two CCD cameras. Adjust the nanopositioner to establish coupling from the fiber taper to the microcavity.
6. Scan the laser wavelength as to obtain an appropriate resonance dip on the oscilloscope.

5. Nanoparticle Detection

To acquire data: Configure the oscilloscope's trigger settings and, using homemade software, collect oscilloscope traces for further processing.

1. Record the data for the buffer solution as a reference.
2. Record the data for the nanoparticle solutions from lowest to highest concentration.
3. Observe the frequency shifts that take place due to nanoparticle binding on the microcavity.

6. Post-Processing of Data

The collected data can be further processed by a self-written MATLAB program. The program should:

1. Read the reference interferometer traces and conduct a least-square fit to the sinusoidal curves. The phases of the fitted sinusoidal are used to estimate the laser jitter on the fly.
2. Read the cavity transmission traces and conduct a least-square fit to the double-Lorentzian function. Optical frequencies corresponding to the resonance dips (v_1, v_2) and their full widths at half maximum (FWHM's, represented by δv_1,δv_2) are determined by comparing the transmission signal to the interferometer signal.
3. Obtain the quality factor of each individual dip from $Q_i = v_i / \delta v_i$, where i can either be 1 (left resonance) or 2 (right resonance).
4. Calculate, as is conventional, the optical frequencies of the resonance dips via the laser scan-voltage, where the laser jitter yields larger measurement noise.
5. Collect the average resonance frequency $v_{avg} = (v_1 + v_2) / 2$ and split frequency $\Delta v = v_2 - v_1$ for each measurement and plot them as a function of time. When a nanoparticle binds onto the surface of the microcavity, sudden shifts of both average resonance frequency and split frequency should be observed.

Representative Results

After following the protocol, the traces can be compiled and fitted. **Figure 3a** shows the typical resonance structure of the microsphere as presented in the video, for which frequency splitting is observed in a DPBS medium. A least-square fit to the double-Lorentzian function indicates that the quality factor of the left and right resonance dips are respectively 2.1×10^8 and 3.8×10^8 in an aqueous environment. The optical frequencies of the FWHM are obtained by comparing the cavity spectrum with the interferometer signal in **Figure 3b,** which yields a high-resolution measurement for the Q. Note that the resonance spectrum is obtained when the laser wavelength is blue shifted, while a red shift measurement yields similar Q values. **Figure 4** shows the resonance spectrograms that can be produced, wherein a double-Lorentzian fit of the transmission curves was computed. In terms of calibration, the laser jitter noise is extracted from the original reference interferometer and subsequently removed from both the interferometer and the microsphere signals. In the absence of laser jitter cancelation, **Figure 4a** simply depicts a spectrogram generated by triggering on resonance valleys. Thermal drift emerges upon calibration, as seen in **Figure 4c**. As opposed to free-space interferometry, the elucidated measurement approach has decreased losses and can conceivably be integrated onto a system-on-chip platform. Quantitatively, FSR measurements for free-space interferometry systems can reach an RMS error of 180 kHz for a cavity $Q = 1.5 \times 10^8$, translating to a relative precision of 5.5×10^{-6} for an FSR = 32.9382 GHz [14].

Figure 5 illustrates continuous tracking of the microcavity's average resonance wavelength for a time period of two-thirds of a minute in the case of DPBS immersion. The gray curve shows that, when the resonance wavelength is obtained by the conventional laser scan-voltage method and the laser jitter is not calibrated out, there is a measured wavelength fluctuation on the order of tens of femtometers. Using a reference interferometer (green curve), the noise is reduced to the subfemtometer regime. Improvements brought on by thermal stabilization are also provided in **Figure 5a** to gauge the subfemtometer noise contributions from an uncooled equivalent (red curve). Meanwhile, a measurement of split frequency yields a similar noise floor to that of the average resonance curve. Evaluations of laser frequency scan rate serve as a by-product of the conferred reference interferometry scheme. As is shown in **Figure 5c**, the laser scan rate fluctuations are on the order of 10 GHz/sec. This may be further attributed to the measurement noise associated with the conventional method; however, this will be suppressed by the reference interferometer. Events indicating the binding of 50 nm polystyrene beads can be further captured using a microsphere, as catalogued in the attached video. The steps for both average resonance and split frequency shifts are clearly visible.

In another published demonstration[2], **Figure 6a** displays the binding of 12.5 nm, 25 nm, and 50 nm radius polystyrene beads diluted in DPBS on a silica microtoroid. As can be seen, this technique yields similar sensitivity enhancements. Further consistent steps for the average resonance and split frequencies are observed in **Figure 6b** for 12.5 nm radius bead binding on a microtoroid surface.

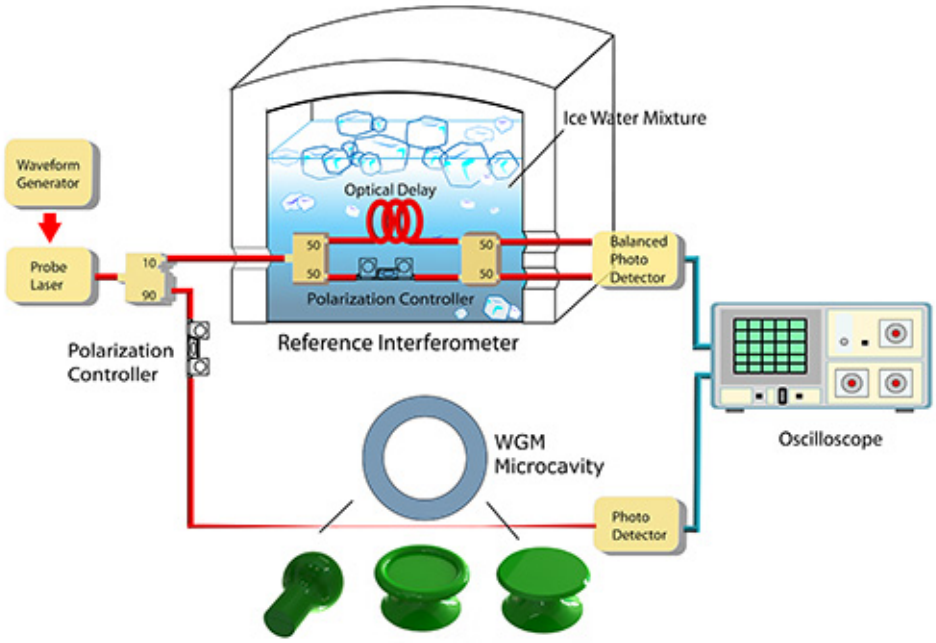

Figure 1. Conceptual diagram of the parallel fiber interferometer configuration, partly comprising images of silica microsphere, microtoroid, and microdisk structures. Please click here to view a larger version of this figure.

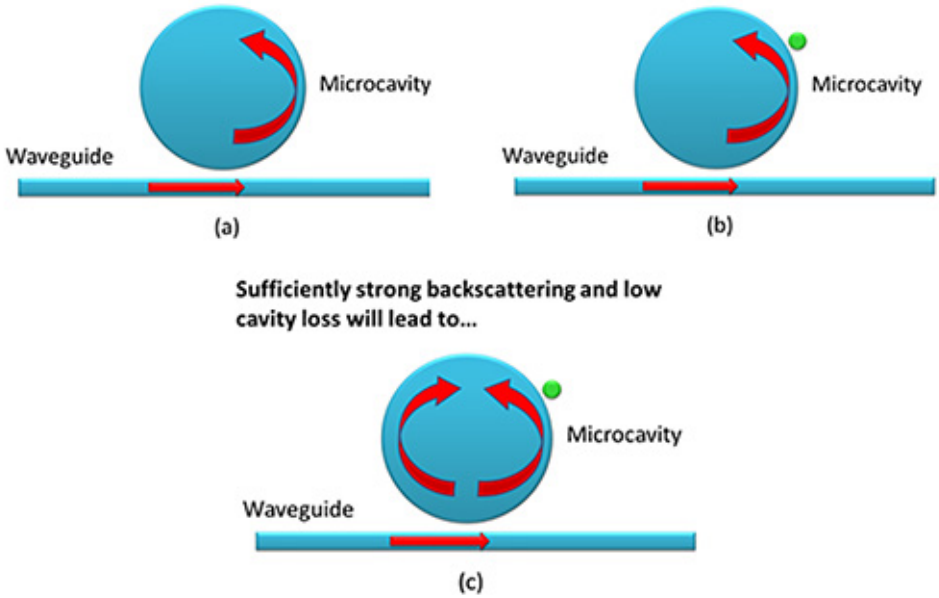

Figure 2. Whispering-gallery mode sensing mechanism: a) Photons are circulating within the microcavity in the absence of nanoparticle binding; **b**) A nanoparticle adsorbs to the surface and is subsequently sampled by the photons, causing perceptible change in optical properties; **c**) Frequency splitting occurs due to the satisfied backscattering and cavity loss conditions, providing an additional dimension to the nanoparticle detection methodology. Please click here to view a larger version of this figure.

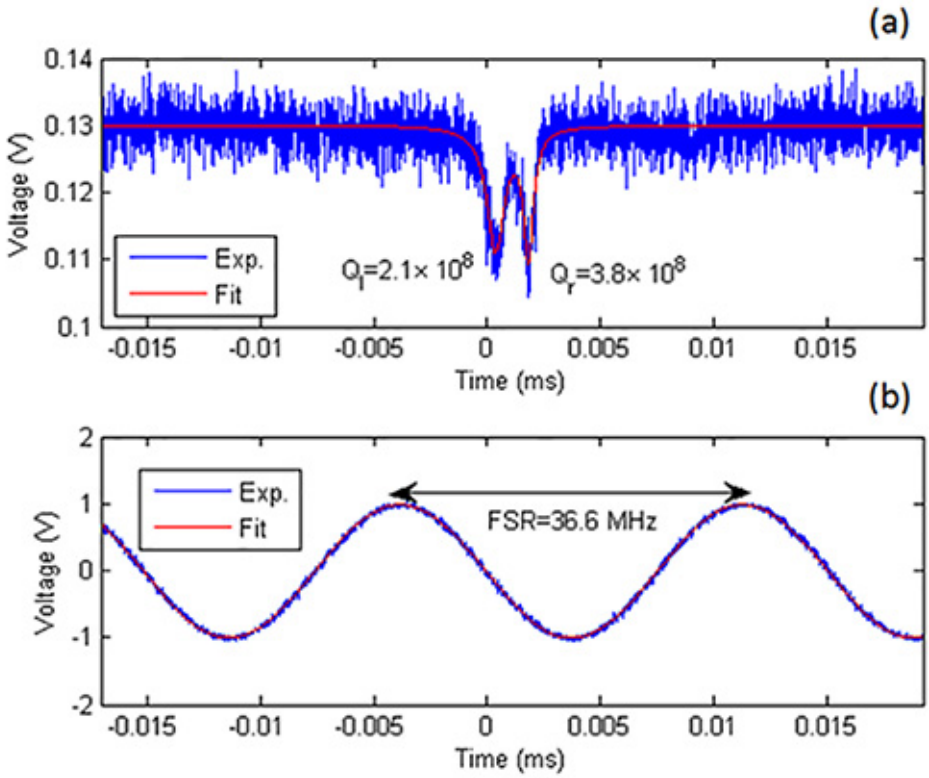

Figure 3. a) An example of a cavity transmission spectrum, showing quality factors of 2.1 x 10^8 for the resonance to the left and 3.8 x 10^8 for the resonance to the right; b) Interferometer signal used to determine the FWHM. Please click here to view a larger version of this figure.

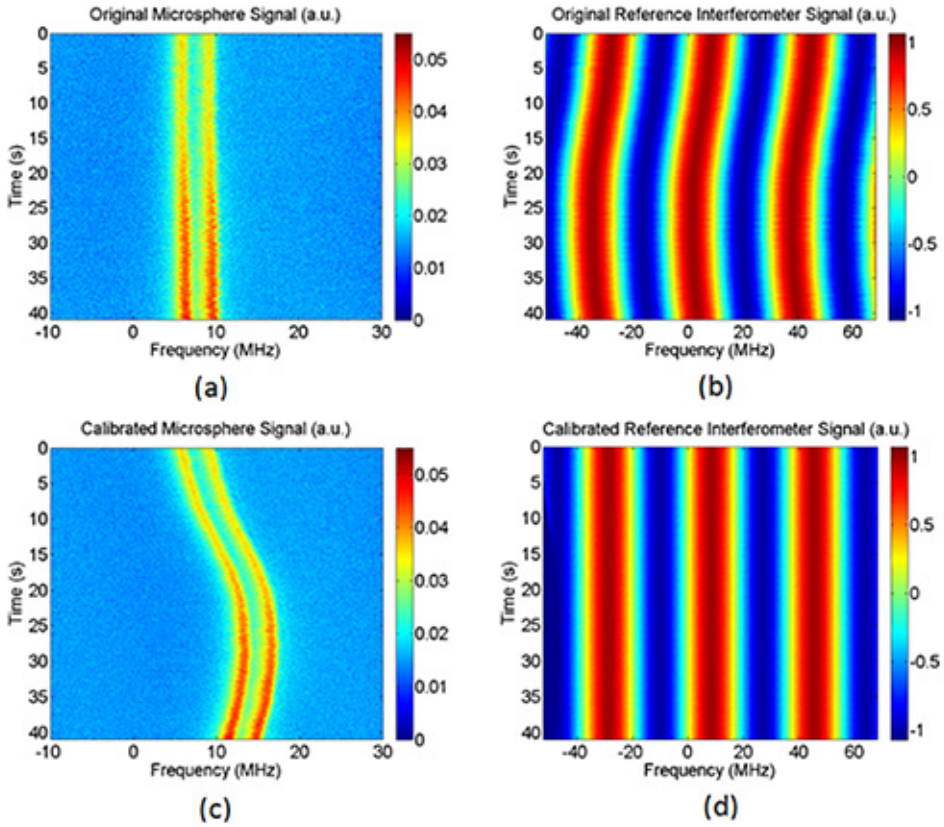

Figure 4. Anticipated raw and sensitivity-enhanced signal spectrograms for the buffer solution. Please click here to view a larger version of this figure.

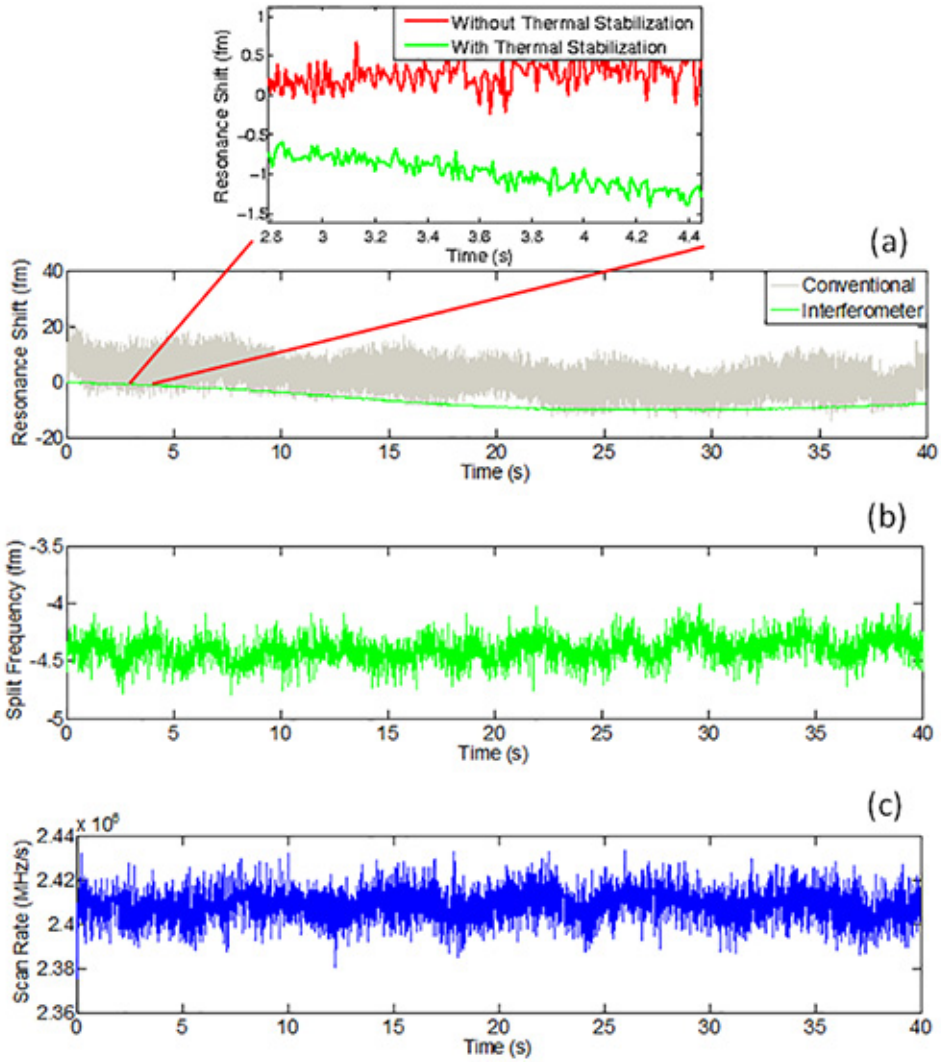

Figure 5. a) Plot of resonant wavelength shift vs. time as well as the discrepancies between excluding (red signal) and including (green signal) thermal stabilization; b) Related time-dependent split frequency; **c**) Related time-dependent scan rate. The first subfigure depicts a gray trace that corresponds to the data for the conventional sweep voltage method, while the green trace is acquired for the reference interferometry technique. Here, the red and green curves located above were recorded on separate dates. Please click here to view a larger version of this figure.

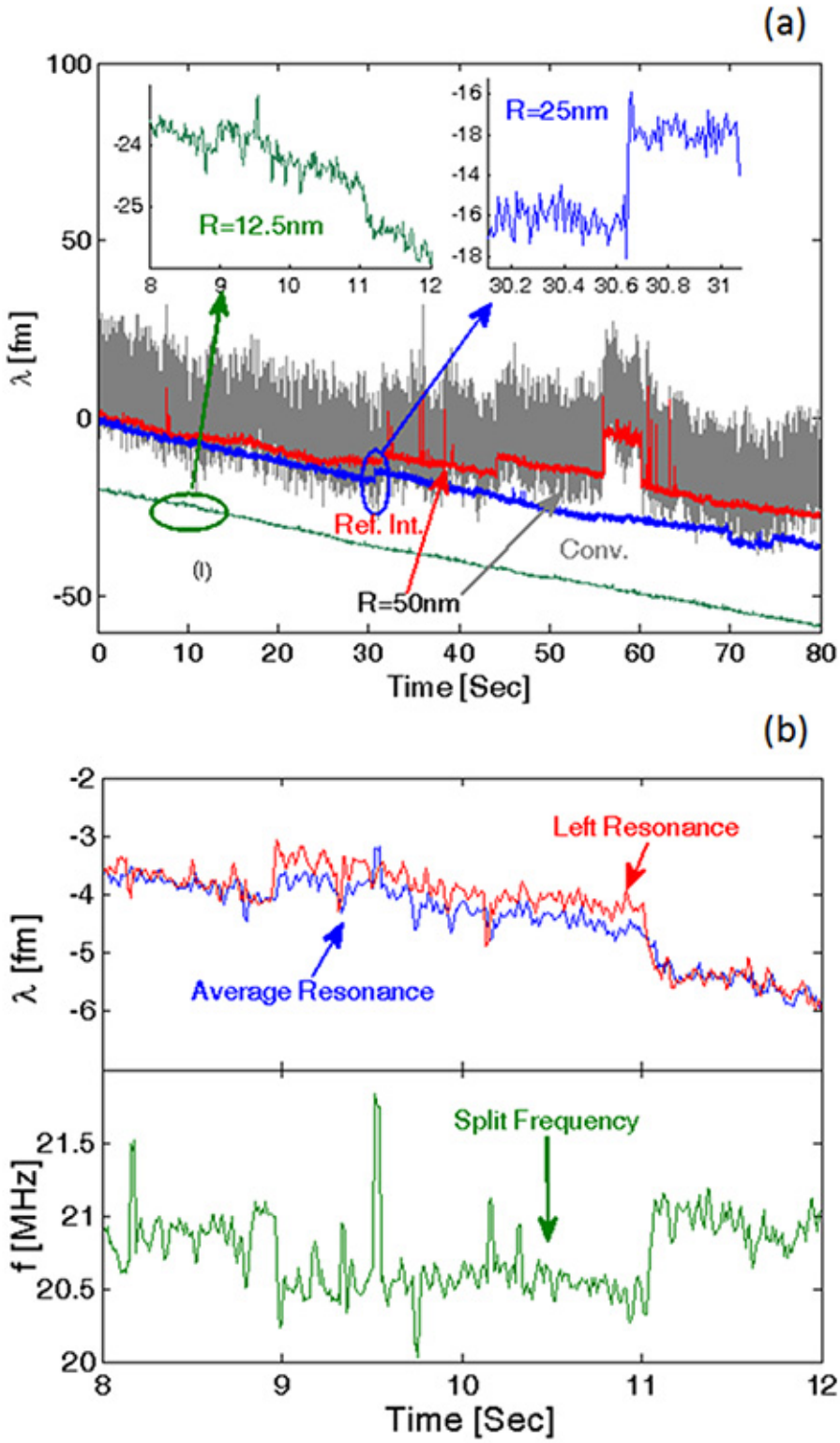

Figure 6. a) Collected average resonance shift steps for 50 nm (red curve), 25 nm (blue curve), and 12.5 nm (green curve) radius beads binding to silica microtoroids; b) Consistent average resonance shift (upper inset) and split frequency shift steps (lower inset), which are observed for 12.5 nm polystyrene beads binding to a microtoroid surface. This figure has been derived from Lu *et al.*[2] Please click here to view a larger version of this figure.

Discussion

This current setup is capable of probing a variety of WGM microcavities, such as microdisks, microspheres, and microtoroids, without requiring any feedback control for the probe laser source. A considerable signal-to-noise ratio (SNR) for detection can be obtained due to the step shift enhancements provided by path length and particle-induced backscattering effects. Given the simplicity and low cost of the reference interferometer itself, this method is an efficient technique for studying or exploiting the properties of WGM cavities.

Alternatively, the power circulating in the microcavity can be optimized and resonance can be more effectively perpetuated via adopting phase modulation (PM) based Pound-Drever-Hall (PDH) frequency locking and amplitude modulation (AM) based critical coupling feedback[15]. This, however, comes at the cost of introducing appreciable complexity and expenditures. Noise floors for the PDH approach have also recently lied around 7 fm [16], raising the noise figure by at least an order of magnitude as compared to the design detailed in this protocol. The nanoparticle scattering cross sections could, as exhibited in trials, be measured through interferometer dissipation information given by cavity enhanced amplitude modulation laser absorption spectroscopy (CEAMLAS)[17].

It is important to note that improperly degased solutions may contain air bubbles of comparable diameter to that of the nanoparticle specimens. More specifically, adsorption of such bubbles to the surface of the microcavity will give rise to false positives in the form of frequency shifting. Such artifacts are difficult to distinguish from the expected signal responses stemming from nanobead binding. Other considerations include the stable flow of liquids near the taper to avoid severing, as well as establishing repeatable fiber taper pulling conditions as to reliably achieve reasonable integrity and insertion loss (≈0.5 dB).

In the past, the biosensing capabilities of this experimental system have been tested by measuring binding for unlabeled influenza A virions in DPBS. The SNR for this particular scenario was reported to be 38:1. The system's potential to detect polystyrene nanobeads with radii as small as 12.5 nm has additionally been demonstrated[2]. Overall, the primary advantage of the reference interferometer based detection methodology lies in its ability to monitor wavelength shifts in real time while minimizing error contributions from frequency jitter and laser scan-voltage control. For instance, removing the jitter noise will alone increase the SNR by a factor of 10. The placement of plasmonic hot spots (*i.e.* bound plasmonic nanoparticles, such as gold nanoshells) on the equator of the WGM cavity in the vicinity of the evanescent field is another means to enhance the detection signal by little over one order of magnitude, without heavily degrading the quality factor[18,19].

Disclosures

The authors have nothing to disclose.

Acknowledgements

The authors would like to thank Xuan Du for constructing the conceptual diagram of **Figure 1.** This work was funded by grants from the Natural Science and Engineering Research Council (NSERC) of Canada.

References

1. Vahala, K. J. Optical microcavities. *Nature.* **424** (6950), 839-846 (2003).
2. Lu, T., *et al.* High sensitivity nanoparticle detection using optical microcavities. *PNAS.* **108** (15), 5976-5979 (2011).
3. Vollmer, F., Arnold, S. Whispering-gallery-mode biosensing: label-free detection down to single molecules. *Nat. Methods.* **5** (7), 591-596 (2008).
4. Vollmer, F., Braun, D., Libchaber, A., Khoshsima, M., Teraoka, I., Arnold, S. Protein detection by optical shift of a resonant microcavity. *Appl. Phys. Lett.* **80** (21), 4057-4059 (2002).
5. Sun, Y., Fan, X. Optical ring resonators for biochemical and chemical sensing. *Anal. Bioanal. Chem.* **399** (1), 205-211 (2011).
6. Shopova, S. I., Rajmangal, R., Nishida, Y., Arnold, S. Ultrasensitive nanoparticle detection using a portable whispering gallery mode biosensor driven by a periodically poled lithium-niobate frequency doubled distributed feedback laser. *Rev. Sci. Instrum.* **81** (10), 103-110 (2010).
7. Santiago-Cordoba, M. A., Boriskina, S. V., Vollmer, F., Demirel, M. C. Nanoparticle-based protein detection by optical shift of a resonant microcavity. *Appl. Phys. Lett.* **99** (7), 073701 (2011).
8. Swaim, J. D., Knittel, J., Bowen, W. P. Detection limits in whispering gallery biosensors with plasmonic enhancement. *Appl. Phys. Lett.* **99** (24), 243109 (2011).
9. Gorodetsky, M. L., Pryamikov, A. D., Ilchenko, V. S. Rayleigh scattering in high-Q microspheres. *J. Opt. Soc. Am. B.* **17** (6), 1051-1057 (2000).
10. Lu, T., Su, J., Fraser, S., Vahala, K. J. *Split frequency sensing methods and systems*. Patent granted on Nov. 26, 2013. Patent No.: US 8,593,638 B2. Provisional application filed on Oct. 2 (2008).
11. Zhu, J., *et al.* On-chip single nanoparticle detection and sizing by mode splitting in an ultrahigh-Q microresonator. *Nat. Photonics.* **4** (1), 46-49 (2010).
12. Shopova, S. I., Rajmangal, R., Nishida, Y., Arnold, S. Ultrasensitive nanoparticle using a portable whispering gallery mode biosensor driven by a periodically poled lithium-niobate frequency doubled distributed feedback laser. *Rev. Sci. Instrum.* **81** (10), 103110 (2010).
13. Cai, M., Painter, O., Vahala, K. J. Observation of critical coupling in a fiber taper to a silica-microsphere whispering-gallery mode system. *Phys. Rev. Lett.* **85** (1), 74-77 (2000).

14. Li, J., Lee, H., Yang, K. Y., Vahala, K. J. Sideband spectroscopy and dispersion measurement in microcavities. *Opt. Express.* **20** (24), 26337-26344 (2012).
15. Chow, J. H., *et al.* Critical coupling control of a microresonator by laser amplitude modulation,*Opt. Express.* **20** (11), 12622-12630 (2012).
16. Swaim, J. D., Knittel, J., Bowen, W. P. Detection of nanoparticles with a frequency locked whispering gallery mode microresonator. *Appl. Phys. Lett.* **102** (18), 183106 (2013).
17. Knittel, J., Chow, J. H., Gray, M. B., Taylor, M. A., Bowen, W. P. Ultrasensitive real-time measurement of dissipation and dispersion in a whispering-gallery mode microresonator. *Opt. Lett.* **38** (11), 1915-1917 (2013).
18. Shopova, S. I., Rajmangal, R., Holler, S., Arnold, S. Plasmonic enhancement of a whispering-gallery-mode biosensor for single nanoparticle detection. *Appl. Phys. Lett.* **98** (24), 243104 (2011).
19. Santiago-Cordoba, M. A., Boriskina, S. V., Vollmer, F., Demirel, M. C. Nanoparticle-based protein detection by optical shift of a resonant microcavity. *Appl. Phys. Lett.* **99** (7), 073701 (2011).

